

Numerical Simulation of Wake-Field Acceleration Using an Eulerian Vlasov Code

M. Shoucri*

Institut de recherche d'Hydro-Québec (IREQ), Varennes, Québec, J3X 1S1, Canada.

Received 9 November 2007; Accepted (in revised version) 15 February 2008

Available online 21 April 2008

Abstract. We study the generation of nonlinear plasma wake fields by intense laser pulses, using an Eulerian code for the numerical solution of the fully relativistic one-dimensional (1D) Vlasov-Maxwell equations. The examination of the phase-space of the distribution function allows to study without numerical noise aspects of the particle acceleration by the wake-field generated by intense laser pulses, in the very low density regions of the phase-space. We study the effect of the thermal spread on the existence of accelerated beams, and we compare between results obtained from a circularly polarized wave and a linearly polarized wave.

PACS: 52.65.Ff

Key words: Eulerian code, Vlasov-Maxwell, wake-field, plasma.

1 Introduction

Large amplitude wake fields can be produced by propagating ultrahigh power, short laser pulses in underdense plasmas. When the laser power is high enough, the electron oscillation (quiver) velocity becomes relativistic, and large amplitude wake fields are generated which support acceleration gradients much greater than those obtained in conventional linear accelerators. Some important aspects of this problem and other nonlinear problems related to large amplitude laser-plasma interactions have been discussed using the cold relativistic fluid equations [1, 2] (see also the review article in [3]).

Numerical simulations however remain the only alternative to study the kinetic effects in this highly relativistic and highly nonlinear problem. Kinetic effects (e.g., particle trapping and acceleration) in short-pulse laser-plasma interactions are often simulated numerically using particle-in-cell (PIC) codes. However several numerical effects in PIC codes can lead to phase-space errors and unphysical numerical heating in the simulation,

*Corresponding author. *Email address:* shoucri.magdi@ireq.ca (M. Shoucri)

and hence the detailed phase-space structure and kinetic effects will be poorly approximated in the simulation. It was indeed reported in [4] that the results obtained by the PIC codes show a momentum spread inside the laser pulse which is excessively and unphysically large. At a high laser intensity, this can lead to spurious trapping of erroneously large levels. The correction of this momentum spread error may require unacceptably high resolution in a PIC code, especially if we want to look beyond the bulk fields for phenomena which depends on the details of the phase-space, especially in the low density regions. A warm fluid model has been presented to study laser-plasma interactions in [4], and in the results reported the bulk fields were insensitive to the details of the distribution functions, for the set of parameters used. This was explained by the fact the Lorentz force was much more important than the pressure force at the temperatures considered. However, many processes of interest, like the trapping and acceleration of a beam, should depend on the details of the phase-space.

We study in the present work the problem of the laser wake-field acceleration by using an Eulerian Vlasov code for the direct numerical solution in phase-space of the 1D relativistic Vlasov-Maxwell equations. Eulerian Vlasov codes have been successfully applied in recent years to study several problems in plasma physics, especially problems associated with wave-particle interaction and stimulated Raman scattering [5]. Interest in Eulerian grid-based Vlasov solvers arise from the very low noise level associated with these codes, which allows accurate representation of the low density regions of the phase-space. This is obviously important if the physics of interest is in the low density region of phase-space or in the high energy tail of the distribution function, as is the case in the present problem. In the laser wake-field accelerator concept, a correctly placed trailing electron bunch can be accelerated by the longitudinal electric field and focused by the transverse electric field of the wake plasma waves. A fully nonlinear 1D relativistic Vlasov-Maxwell model to study the self-consistent interaction of intense laser pulses with plasmas can be found for instance in [6]. A characteristic parameter of a high power laser beam is the normalized vector potential

$$|\vec{\alpha}_\perp| = |e\vec{A}_\perp / M_e c^2| = \alpha_0,$$

where \vec{A}_\perp is the vector potential, e and M_e the electronic charge and mass respectively, and c the speed of light. We are interested in the regime $\alpha_0 \geq 1$.

A problem related to the laser wake-field accelerator concept is the plasma wake-field accelerator, where the plasma responds to the self-fields of a driving electron beam, instead of the ponderomotive forces of the laser pulse. The problem of the plasma wake-field accelerator has been studied using an Eulerian Vlasov code to solve the 1D relativistic Vlasov-Maxwell equations [7]. The numerical technique was based on a fractional step method similar to what has been presented in [8,9]. This numerical approach differs from the one we use in the present work, which consists of integrating the Vlasov equation along its characteristics in two dimensions, using a tensor product of cubic B-splines for the interpolation along the characteristics, without applying a fractional step technique [10]. A kinetic equation for the ions is included in the simulations.

2 The relevant equations

2.1 The 1D relativistic Vlasov-Maxwell model

Time t is normalized to the inverse electron plasma frequency ω_{pe}^{-1} , length is normalized to $l_0 = c\omega_{pe}^{-1}$, velocity and momentum are normalized respectively to the velocity of light c and to $M_e c$. The general form of the Vlasov equation in a 4D phase-space for the electron distribution function $F_e(x, p_{xe}, p_{ye}, p_{ze}, t)$ and the ion distribution function $F_i(x, p_{xi}, p_{yi}, p_{zi}, t)$ (one spatial dimension) is written in a dimensionless form as follows :

$$\frac{\partial F_{e,i}}{\partial t} + m_{e,i} \frac{p_{xe,i}}{\gamma_{e,i}} \frac{\partial F_{e,i}}{\partial x} \mp \left(\vec{E} + \frac{\vec{p} \times \vec{B}}{\gamma_{e,i}} \right) \cdot \frac{\partial F_{e,i}}{\partial \vec{p}_{e,i}} = 0, \quad (2.1)$$

with

$$\gamma_{e,i} = \left(1 + m_{e,i}^2 \left(p_{xe,i}^2 + p_{ye,i}^2 + p_{ze,i}^2 \right) \right)^{1/2}, \quad (2.2)$$

(the upper sign in (2.1) is for the electrons equation and the lower sign for the ions equation, and subscripts e or i denote electrons or ions respectively). In our normalized units $m_e = 1$ and $m_i = M_e / M_i$, the ratio of electron to ion masses.

We write the Hamiltonian of a particle in the electromagnetic field of the wave:

$$H_{e,i} = \frac{1}{m_{e,i}} (\gamma_{e,i} - 1) \mp \varphi, \quad (2.3)$$

where φ is the scalar potential. Eq. (2.1) can be reduced to a two-dimensional phase-space Vlasov equation as follows. The canonical momentum $\vec{P}_{ce,i}$ is connected to the particle momentum $\vec{p}_{e,i}$ by the relation

$$\vec{P}_{ce,i} = \vec{p}_{e,i} \mp \vec{\alpha},$$

where $\vec{\alpha} = e\vec{A} / M_e c$ is the normalized vector potential. From Eqs. (2.2)-(2.3), we can write

$$H_{e,i} = \frac{1}{m_{e,i}} \left(\left(1 + m_{e,i}^2 \left(\vec{P}_{ce,i} \pm \vec{\alpha} \right)^2 \right)^{1/2} - 1 \right) \mp \varphi. \quad (2.4)$$

Choosing the Coulomb gauge ($\text{div} \vec{\alpha} = 0$), we have for our 1D problem $\partial \alpha_x / \partial x = 0$, hence $\alpha_x = 0$. The vector potential is now $\vec{\alpha} = \vec{\alpha}_\perp(x, t)$, and we also have the following relation along the longitudinal direction:

$$\frac{dP_{cxe,i}}{dt} = - \frac{\partial H_{e,i}}{\partial x}. \quad (2.5)$$

And since there is no transverse dependence:

$$\frac{d\vec{P}_{c\perp e,i}}{dt} = - \nabla_\perp H_{e,i} = 0. \quad (2.6)$$

This last equation means $\vec{P}_{c\perp e,i} = \text{const}$. We can choose this constant to be zero without loss of generality, which means that initially all particles at a given (x, t) have the same perpendicular momentum $\vec{p}_{\perp e,i} = \pm \vec{\alpha}_{\perp}(x, t)$. The Hamiltonian now is written:

$$H_{e,i} = \frac{1}{m_{e,i}} \left((1 + m_{e,i}^2 p_{xe,i}^2 + m_{e,i}^2 \alpha_{\perp}^2(x, t))^{1/2} - 1 \right) \mp \varphi(x, t). \quad (2.7)$$

The 4D distribution function $F_{e,i}(x, p_{xe,i}, \vec{p}_{\perp e,i}, t)$ can now be reduced to a 2D distribution function $f_{e,i}(x, p_{xe,i}, t)$:

$$F_{e,i}(x, p_{xe,i}, \vec{p}_{\perp e,i}, t) = f_{e,i}(x, p_{xe,i}, t) \delta(\vec{p}_{\perp e,i} \mp \vec{\alpha}_{\perp}), \quad (2.8)$$

where $f_{e,i}(x, p_{xe,i}, t)$ verify the relation:

$$\frac{\partial f_{e,i}}{\partial t} = \frac{\partial f_{e,i}}{\partial t} + \frac{\partial H_{e,i}}{\partial p_{xe,i}} \frac{\partial f_{e,i}}{\partial x} - \frac{\partial H_{e,i}}{\partial x} \frac{\partial f_{e,i}}{\partial p_{xe,i}} = 0. \quad (2.9)$$

This gives the following Vlasov equations for the electrons and the ions:

$$\frac{\partial f_{e,i}}{\partial t} + m_{e,i} \frac{p_{xe,i}}{\gamma_{e,i}} \frac{\partial f_{e,i}}{\partial x} + \left(\mp E_x - \frac{m_{e,i}}{2\gamma_{e,i}} \frac{\partial \alpha_{\perp}^2}{\partial x} \right) \frac{\partial f_{e,i}}{\partial p_{xe,i}} = 0. \quad (2.10)$$

where

$$\begin{aligned} \gamma_{e,i} &= (1 + (m_{e,i} p_{xe,i})^2 + (m_{e,i} \alpha_{\perp})^2)^{1/2}, \\ E_x &= -\frac{\partial \varphi}{\partial x}, \quad \vec{E}_{\perp} = -\frac{\partial \vec{\alpha}_{\perp}}{\partial t}, \end{aligned} \quad (2.11)$$

and Poisson's equation is given by

$$\frac{\partial^2 \varphi}{\partial x^2} = \int f_e(x, p_{xe}) dp_{xe} - \int f_i(x, p_{xi}) dp_{xi}. \quad (2.12)$$

The transverse electromagnetic fields E_y, B_z and E_z, B_y for the circularly polarized wave obey Maxwell's equations. With $E^{\pm} = E_y \pm B_z$ and $F^{\pm} = E_z \pm B_y$, we have

$$\left(\frac{\partial}{\partial t} \pm \frac{\partial}{\partial x} \right) E^{\pm} = -J_y; \quad \left(\frac{\partial}{\partial t} \mp \frac{\partial}{\partial x} \right) F^{\pm} = -J_z, \quad (2.13)$$

which are integrated along their vacuum characteristic $x = t$. In our normalized units we have the following expressions for the normal current densities:

$$\vec{J}_{\perp} = \vec{J}_{\perp e} + \vec{J}_{\perp i}; \quad \vec{J}_{\perp e,i} = -\vec{\alpha}_{\perp} m_{e,i} \int_{-\infty}^{+\infty} \frac{f_{e,i}}{\gamma_{e,i}} dp_{xe,i}. \quad (2.14)$$

2.2 The numerical scheme

Since the early works presented in [8, 9] which proposed the second-order fractional step scheme for the solution of the Vlasov-Poisson system, the direct solution of the Vlasov equation as a partial differential equation in phase-space has become an important method for the numerical solution of the Vlasov equation (see the review articles in [11, 12]). The code we use applies a numerical scheme based on a two-dimensional advection technique, of second order accuracy in time-step, where the value of the distribution function is advanced in time by interpolating in two dimensions along the characteristics using a tensor product of cubic *B*-splines [13, 14], also called an Euler-Lagrange method [15].

The numerical scheme to advance equation (2.10) from time t_n to t_{n+1} necessitates the knowledge of the electromagnetic field E^\pm and F^\pm at time $t_{n+1/2}$. This is done using a centered scheme where we integrate (2.13) exactly along the vacuum characteristics with $\Delta x = \Delta t$, to calculate $E^{\pm n+1/2}$ and $F^{\pm n+1/2}$ as follows:

$$E^\pm(x \pm \Delta t, t_{n+1/2}) = E^\pm(x, t_{n-1/2}) - \Delta t J_y(x \pm \Delta t/2, t_n), \tag{2.15}$$

with

$$J_y(x \pm \Delta t/2, t_n) = \frac{J_y(x \pm \Delta x, t_n) + J_y(x, t_n)}{2}.$$

A similar equation can be written for $F^{\pm n+1/2}$. From (2.11) we also have

$$\vec{\alpha}_\perp^{n+1} = \vec{\alpha}_\perp^n - \Delta t \vec{E}_\perp^{n+1/2},$$

from which we calculate

$$\vec{\alpha}_\perp^{n+1/2} = \frac{1}{2}(\vec{\alpha}_\perp^{n+1} + \vec{\alpha}_\perp^n).$$

To calculate $E_x^{n+1/2}$, two methods have been used. A first method calculates E_x^n from $f_{e,i}^n$ using Poisson's equation, then we use a Taylor expansion:

$$E_x^{n+1/2} = E_x^n + \frac{\Delta t}{2} \left(\frac{\partial E_x}{\partial t} \right)^n + 0.5 \left(\frac{\Delta t}{2} \right)^2 \left(\frac{\partial^2 E_x}{\partial t^2} \right)^n; \tag{2.16}$$

with

$$\left(\frac{\partial E_x}{\partial t} \right)^n = -J_x^n; \quad \left(\frac{\partial^2 E_x}{\partial t^2} \right)^n = - \left(\frac{\partial J_x}{\partial t} \right)^n,$$

$$J_x^n = m_i \int_{-\infty}^{+\infty} \frac{p_{xi}}{\gamma_i} f_i^n dp_{xi} - m_e \int_{-\infty}^{+\infty} \frac{p_{xe}}{\gamma_e} f_e^n dp_{xe}.$$

A second method to calculate $E_x^{n+1/2}$ is to use Ampère's equation: $\partial E_x / \partial t = -J_x$, from which

$$E_x^{n+1/2} = E_x^{n-1/2} - \Delta t J_x^n.$$

Both methods gave the same results. (We have used the second method for the results presented in Section 3).

Eq. (2.10) is solved using an Euler-Lagrange scheme. Given $f_{e,i}^n$ at mesh points (we stress here that the subscript i denotes the ion distribution function), we calculate the new value $f_{e,i}^{n+1}$ at the grid points j_x , and j_p corresponding to the mesh points $(x_{j_x}, p_{x_{e,i j_p}})$ by writing that the distribution function is constant along the characteristics. The characteristics equations for (2.10) are given by:

$$\begin{aligned} \frac{dx}{dt} &= m_{e,i} \frac{p_{x_{e,i}}}{\gamma_{e,i}} = V_{x_{e,i}}(x, p_{x_{e,i}}), \\ \frac{dp_{x_{e,i}}}{dt} &= \mp E_x - \frac{m_{e,i}}{2\gamma_{e,i}} \frac{\partial \alpha_{\perp}^2}{\partial x} = V_{p_{x_{e,i}}}(x, p_{x_{e,i}}). \end{aligned} \quad (2.17)$$

We assume that at the time $t_{n+1} \equiv t_n + \Delta t$, x is at the grid point j_x , and $p_{x_{e,i}}$ is at the grid point j_p . The following leapfrog scheme can be written for the solution of (2.17):

$$\frac{x_{j_x} - x(t_n)}{\Delta t} = V_{x_{e,i}}(x^{n+1/2}, p_{x_{e,i}}^{n+1/2}) = V_{x_{e,i}}\left(\frac{x_{j_x} + x(t_n)}{2}, \frac{p_{x_{e,i j_p}} + p_{x_{e,i}}(t_n)}{2}\right), \quad (2.18)$$

$$\frac{p_{x_{e,i j_p}} - p_{x_{e,i}}(t_n)}{\Delta t} = V_{p_{x_{e,i}}}(x^{n+1/2}, p_{x_{e,i}}^{n+1/2}) = V_{p_{x_{e,i}}}\left(\frac{x_{j_x} + x(t_n)}{2}, \frac{p_{x_{e,i j_p}} + p_{x_{e,i}}(t_n)}{2}\right), \quad (2.19)$$

where $(x(t_n), p_{x_{e,i}}(t_n))$ is the point where the characteristic is originating at t_n (not necessarily a grid point). Put

$$\Delta_{x_{e,i}} = \frac{x_{j_x} - x(t_n)}{2}; \quad \Delta_{p_{x_{e,i}}} = \frac{p_{x_{e,i j_p}} - p_{x_{e,i}}(t_n)}{2}. \quad (2.20)$$

Eqs. (2.18)-(2.19) can be rewritten as:

$$\Delta_{x_{e,i}} = \frac{\Delta t}{2} V_{x_{e,i}}(x_{j_x} - \Delta_{x_{e,i}}, p_{x_{e,i j_p}} - \Delta_{p_{x_{e,i}}}), \quad (2.21)$$

$$\Delta_{p_{x_{e,i}}} = \frac{\Delta t}{2} V_{p_{x_{e,i}}}(x_{j_x} - \Delta_{x_{e,i}}, p_{x_{e,i j_p}} - \Delta_{p_{x_{e,i}}}), \quad (2.22)$$

which are implicit equations for $\Delta_{x_{e,i}}$ and $\Delta_{p_{x_{e,i}}}$ and are solved by iteration. This iteration is effected as follows. We rewrite (2.21)-(2.22) in the vectorial form

$$\Delta_{X_{e,i}} = \frac{\Delta t}{2} V_{e,i}(X_{e,i} - \Delta_{X_{e,i}}, t_{n+1/2}), \quad (2.23)$$

where $X_{e,i}$ is the two dimensional vector $X_{e,i} = (x, p_{x_{e,i}})$, and $\Delta_{X_{e,i}} = (\Delta_{x_{e,i}}, \Delta_{p_{x_{e,i}}})$ is the two dimensional vector in (2.23) and

$$V_{e,i} = (V_{x_{e,i}}^{n+1/2}, V_{p_{x_{e,i}}}^{n+1/2}).$$

Eq. (2.23) for $\Delta_{X_{e,i}}$ is implicit and is solved iteratively:

$$\Delta_{X_{e,i}}^{k+1} = \frac{\Delta t}{2} V_{e,i}(X_{e,i} - \Delta_{X_{e,i}}^k, t_{n+1/2}),$$

where we start the iteration with $\Delta_{X_{e,i}}^0 = 0$ for $k = 0$. Usually two or three iterations are sufficient to get a good convergence. The shifted values in (2.21), (2.22) are calculated by a two-dimensional interpolation using a tensor product of cubic B -splines [13, 14]. We now write that the distribution function is constant along the characteristics. Then $f_{e,i}^{n+1}$ is calculated from $f_{e,i}^n$ from the relation:

$$f_{e,i}^{n+1}(x_{j_x}, p_{x_{e,i j_p}}) = f_{e,i}^n(x(t_n), p_{x_{e,i}(t_n)}) = f_{e,i}^n(x - 2\Delta_{x_{e,i}}, p_{x_{e,i}} - 2\Delta_{p_{x_{e,i}}}). \quad (2.24)$$

Again the shifted values in (2.24) are calculated with a two-dimensional interpolation using a tensor product of cubic B -splines. Details have been presented in [11, 13, 14].

3 Results

A generous number of grid points has been used in the simulation, to reproduce accurately the fine details which develop in the phase-space. The fine structure of the accelerated beam requires a fine resolution in the phase-space. For all the results we present, $N_x = 10000$ is the number of grid points in space, for a length $L_x = 40.355$. $N_{pxe} = 1600$ is the number of grid points in momentum for the electrons, and for the ions $N_{pxi} = 256$. The code is executed on a single Opteron 2218 processor at 2.6 Ghz and 8 Gb of main memory. The memory required by the code was 1.6 Gb, and required a CPU time for the execution of about 300 hours up to $t = 40.355$. Parallelization can certainly accelerate this performance, the code is about 2000 lines, however in view of the relatively moderate memory required, several codes with different parameters can be executed simultaneously. (Note that for the results in Fig. 11 for instance, where p_{maxe} can be reduced to 7, the code was run with $N_{pxe} = 800$ in only 80 hours CPU time, with very little differences in the results).

We assume the frequency of the laser pulse $\omega_0/\omega_p \gg 1$ ($\omega_0/\omega_p = 10$ in the present calculation), and the envelope of the laser pulse changes on a time-scale which is long compared to the wave period. The spatial length of the envelope of the laser pulse is $L = \lambda_p = 2\pi c/\omega_p$, much longer than the laser field wavelength λ . The model is similar to what has been presented in [1, 2] with the addition that in the present simulation we include a 1D kinetic relativistic Vlasov equation, and this is done for both electrons and ions. The evolution of the laser pulse is calculated self-consistently with Maxwell's equations. We assume that the laser beam transverse dimension $r \gg \lambda_p$, which is necessary for the validity of the 1D model. The system is initially neutral ($n_e = n_i$). The density in our normalized units is equal to 1 in the flat central part, with steep gradients and vacuum at both ends. The length of the vacuum region is 1.18 on each side, and the length of the transition region for the zero density to the flat density of 1 is 1.41, hence this transition region is about 2.6 on each side.

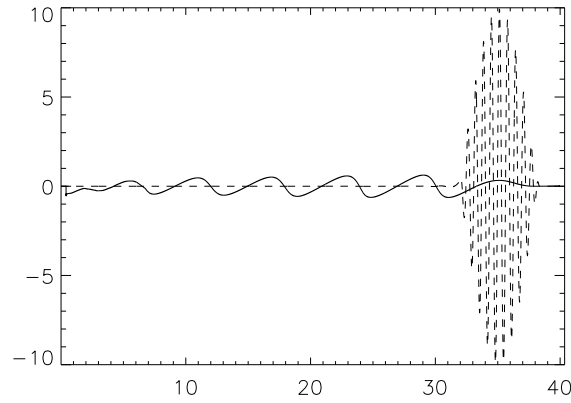


Figure 1: Laser pulse (broken curve) and the wake field E_x (full curve) at $t=38.33$.

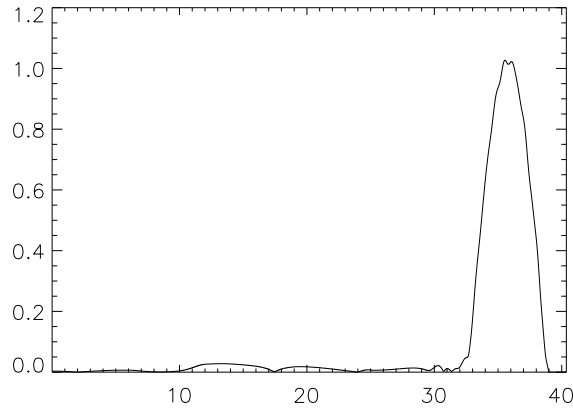


Figure 2: Plot of $a_{\perp} = \sqrt{a_y^2 + a_z^2}$ at $t=38.33$ for the circularly polarized wave.

3.1 The case of a circularly polarized electromagnetic wave

The electrons and ions have initially a Maxwellian distribution. Two cases will be studied. A case with a temperature $T_e = 0.4keV$ for the electrons and $T_i = 0.1keV$ for the ions, and a case with a temperature $T_e = 3keV$ for the electrons and $T_i = 1keV$ for the ions. In both cases we have for the electrons ($p_{xmaxe} = 15$, $p_{xmine} = -15$), and for the ions ($p_{xmaxi} = 10.8$, $p_{xmini} = -10.8$).

The forward propagating circularly polarized laser pulse is penetrating from the vacuum at the left boundary, and propagate towards the right, and is written in our normalized units as:

$$E^+ = 2E_0 \sin(\pi\zeta/L) \sin(k_0\zeta), \quad (3.1)$$

$$F^- = 2E_0 \sin(\pi\zeta/L) \cos(k_0\zeta), \quad (3.2)$$

for $2.6 < t < 2\pi + 2.6$, and for $-L \leq \zeta \leq 0$, $\zeta = x - t$. And $E_0 = 0$ otherwise. 2.6 is the length

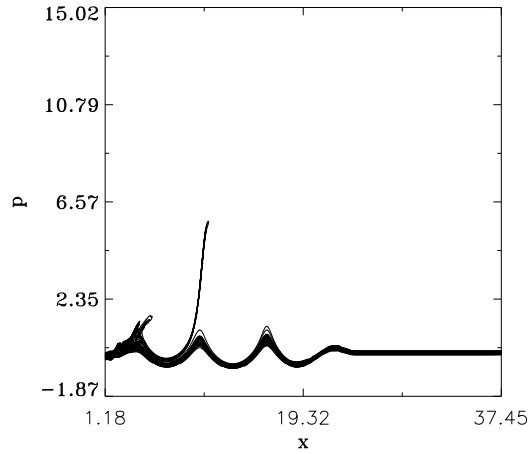


Figure 3: Phase-space contour plot of the electron distribution function at $t=24.21$ for the case with $T_e=0.4keV$, and a circularly polarized wave.

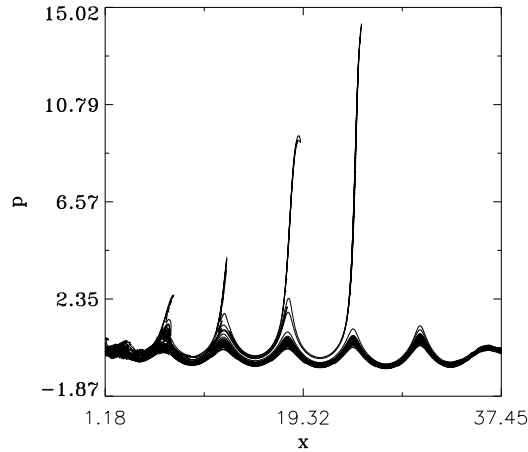


Figure 4: Phase-space contour plot of the electron distribution function at $t=38.33$ for the case with $T_e=0.4keV$, and a circularly polarized wave.

of the vacuum and transition region, as mentioned in the previous section. This allows the pulse to develop on the flat part of the density profile. L is the length of the pulse envelope. In vacuum we have for the electromagnetic (EM) wave $k_0 = \omega_0 = 10$ (so in our normalized units the wavelength $\lambda = 2\pi/k_0 = 0.628$). We have ten oscillations of the EM wave in the length $L = 2\pi$ of the pulse envelope. We choose for the amplitude of the potential vector $\alpha_0 = 1$, so that $E_0 = \omega_0\alpha_0 = 10$. Since the envelope is slowly varying, we can write for the corresponding vector potential for $2.6 < t < 2\pi + 2.6$:

$$\alpha_y = -\alpha_0 \sin(\pi\tilde{\zeta}/L) \cos(k_0\tilde{\zeta}), \quad \alpha_z = \alpha_0 \sin(\pi\tilde{\zeta}/L) \sin(k_0\tilde{\zeta}).$$

At $t = 2\pi + 2.6$, the entire envelope of length $L = 2\pi$ of the forward propagating pulse

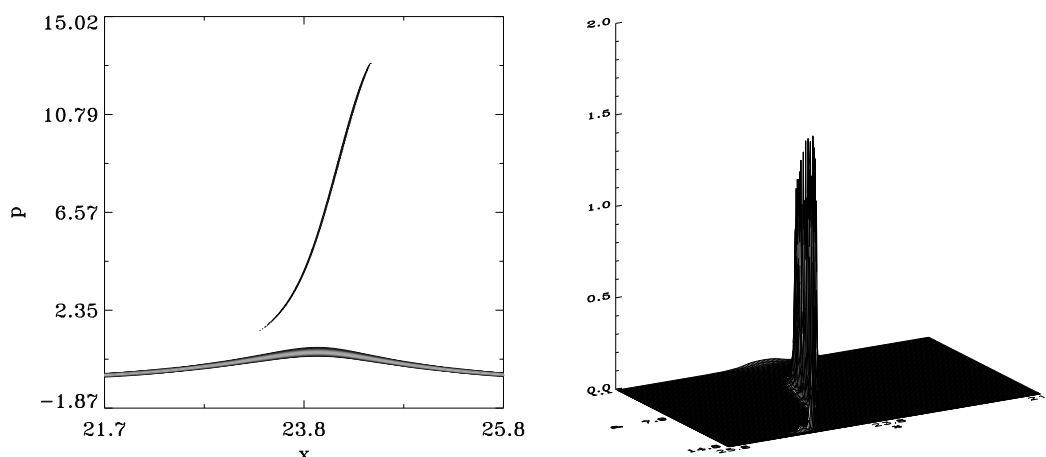


Figure 5: Phase-space contour plot and 3D view of the electron distribution function at $t=38.33$, and at the position of the first accelerated beam at the right of Fig. 4. The 3D view concentrates on the top of the beam tail, and show a very well localized beam structure at the top.

has developed on the flat density part, and is left to evolve self-consistently using (2.13), where $\vec{\alpha}_\perp$ is calculated as indicated in the previous section.

Fig. 1 shows the results for the laser pulse at $t=38.33$ (broken curve), after crossing the domain and reaching the right boundary, which is followed by the wake field E_x (full curve), for the case with a temperature $T_e=0.4keV$ for the electrons and $T_i=0.1keV$ for the ions. For the present set of parameters, the pulse has propagated through the plasma with little deformation. The quantity

$$\alpha_\perp = \sqrt{\alpha_y^2 + \alpha_z^2}$$

which appears in (2.10) is shown in Fig. 2. There is little deformation of the EM pulse for the present set of parameters (see Fig. 1), and since $\sin^2(k_0\zeta) + \cos^2(k_0\zeta) = 1$, then α_\perp defined above is essentially the envelope of the pulse. Figs. 3 and 4 show the phase-space plots for the electrons at $t=24.21$ and $t=38.33$. Bunches of electrons detach from the bulk and are accelerated as beams around the peaks of the electric field. Note that the contour level of the accelerated tail is emphasized in Figs. 3 and 4, in order to make it more visible. Fig. 5 shows a contour plot of the first peak at the right of Fig. 4 without emphasizing the accelerated tail. The 3D view in Fig. 5 concentrates on the top of the long tail and shows clearly a very localized beam at the top of the long tail.

We plot in Figs. 6 and 7 the wake field obtained at $T_e=0.4keV$ (full curves, same as in Fig. 1), and the wake field obtained at a higher temperature, with $T_e=3keV$ (broken curves). The ion temperature for the case with $T_e=3keV$ is $T_i=1keV$. The small bump at the right in Figs. 6 and 7 indicates the position of the EM pulse (see Fig. 1 at $t=38.33$). Just behind the position of the pulse the full curve and the broken curve give essentially the same peaks. The amplitude of E_x reaches, since the beginning of the simulation, a

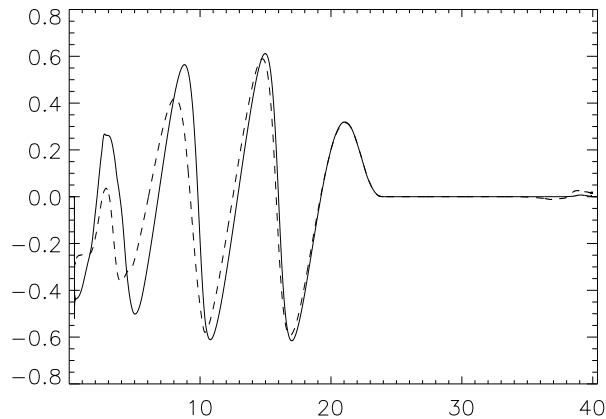


Figure 6: Plot at $t=24.21$ of the axial wake field E_x (full curve for $T_e=0.4keV$ and broken curve for $T_e=3keV$), for the circularly polarized wave.

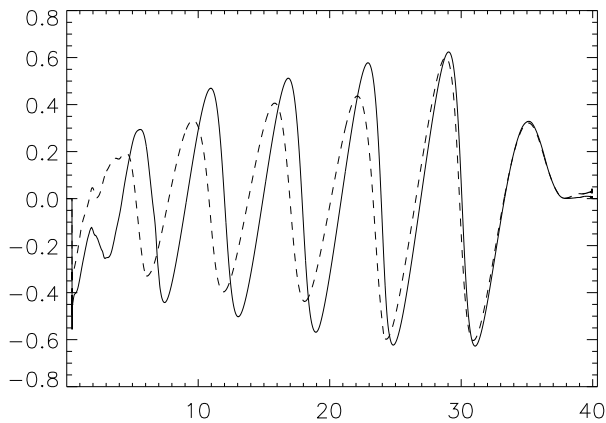


Figure 7: Plot at $t=38.33$ of the axial wake field E_x (full curve for $T_e=0.4keV$ and broken curve for $T_e=3keV$), for the circularly polarized wave.

maximum peak of about 0.63 just behind the pulse (see Fig. 6 at $t=24.21$). This is close to the projected theoretical value for saturation for cold plasma [1,2] given by

$$E_{xmax} = (\gamma_0^2 - 1) / \gamma_0 = 0.717,$$

where $\gamma_0 = \sqrt{1 + \alpha_0^2} = \sqrt{2}$. However, towards the left boundary, the two curves show a small difference in the decreasing peaks and the position of the peaks. The decrease in the peaks is a temperature effect, this decrease seems to be less pronounced when the temperature is reduced. Indeed the results reported for a cold plasma [1,2] showed the electric field reaching a constant amplitude throughout the domain. The present decay of the amplitude of the electric field agrees however with the results reported in [7] for the plasma wake-field accelerators. Note the electric field E_x shows a slightly steeper

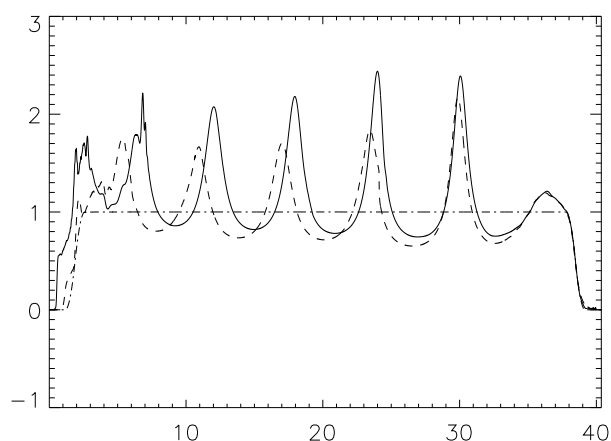


Figure 8: Plot at $t=38.33$ of the electron density (full curve $T_e=0.4keV$ and broken curve for $T_e=3keV$), and the ion density (dash-dot curve) for the circularly polarized wave.

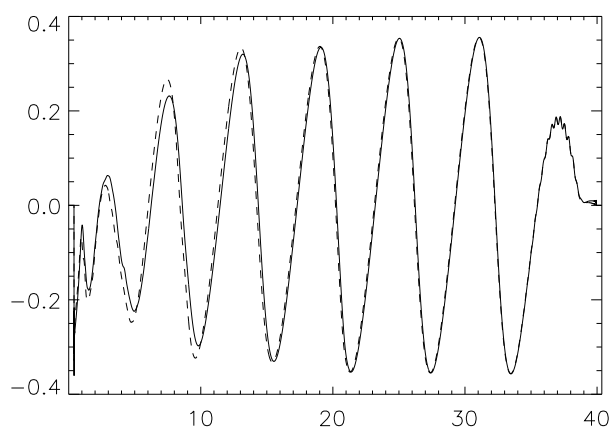


Figure 9: Plot at $t=38.33$ of the axial wake field E_x (full curve for $T_e=0.4keV$ and broken curve for $T_e=0.2keV$), for the linearly polarized wave.

variation at the right of Fig. 6 compared to the profile at the left. The electron density (initially equal to 1 in the flat region of the profile) is forming spikes surrounded by depleted regions (full curve in Fig. 8 for the case $T_e=0.4keV$ and broken curve for the case $T_e=3keV$), and the electric field E_x is rapidly changing sign at these spikes. The dash-dot curve in Fig. 8 is the result obtained for the ions, this profile is essentially unchanged. The density peak just behind the pulse at the right of Fig. 8 is reaching a value of 2.4 for the full curve, and 2.1 for the broken curve. These peak values are reached since the beginning of the simulation, the shape of the density and of the wake field just behind the pulse remain constant during the propagation of the pulse. So the front peaks for both wake field and density seem to be following the laser pulse with little deformation along the flat top of the density profile.

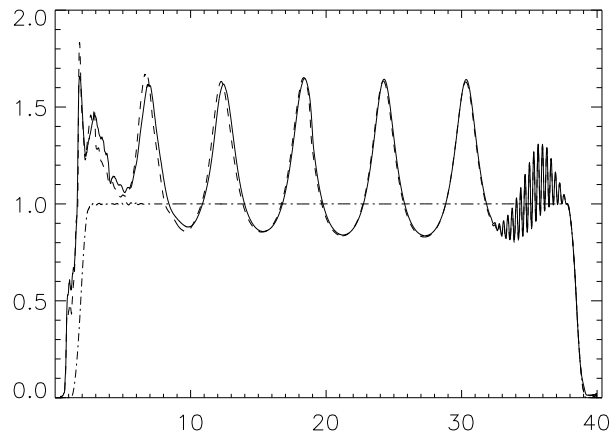


Figure 10: Plot at $t=38.33$ of the electron density (full curve for $T_e=0.4keV$ and dotted curve for $T_e=0.2keV$), and the ion density (dash-dot curve).

3.2 The case of a linearly polarized electromagnetic wave

In this case only E^+ in (3.1) is excited as before and $F^- = 0$. Only α_y is excited initially, then $\alpha_{\perp}^2 = \alpha_y^2$, and α_0 is still the amplitude of the vector potential, except that in this case α_{\perp} is modulated in time. Fig. 9 shows the wake fields for the case $T_e=0.4keV$ (full curve), and the case $T_e=0.2keV$ (broken curve) at $t=38.33$, and Fig. 10 shows the corresponding curves for the density (the dash-dot curve is for the ions density, essentially unchanged). The extrema of the momentum are ± 15 for the first case, and ± 10 for the second case. There is no difference between the full curves and the broken curves in Figs. 9 and 10, and the peaks remain essentially constant behind the pulse, with the exception of those close to the left boundary. The peak electric field is 0.38 (it was 0.63 for the circularly polarized case in Section 3.1). At the right of Fig. 10 the fine scale structure is the result of the quiver motion of the electrons. This fine scale structure due to the quiver motion is also visible in the contour plot of the electron distribution function at the right of Fig. 11, for the linearly polarized case with $T_e=0.4keV$. The first accelerated beam in Fig. 11 appears only at the third peak and is less developed with respect to the one in Fig. 4 for the circularly polarized case (also calculated for $T_e=0.4keV$), at the same time $t=38.33$. The peaks behind the pulse in Figs. 9 and 10 appear more uniform than those in Figs. 7 and 8. Fig. 12 give the contour plot of the ion distribution function at $t=38.33$ for the linearly polarized case with $T_e=0.4keV$ (T_i is $0.1keV$ for this case). It shows a modulation with the same wavelength as for the electron distribution function. However the ion density remained flat in the central region, as indicated in Fig. 10. Finally a simulation with $T_e=0.05keV$ and $T_i=0.01keV$ gave the same results as in Figs. 9 and 10. The wake field E_x and the density appear to depend little on the temperature. The phase-space plot for this case was also close to what is presented in Fig. 11 showing the presence of accelerated beams preceded by fine filament tails.

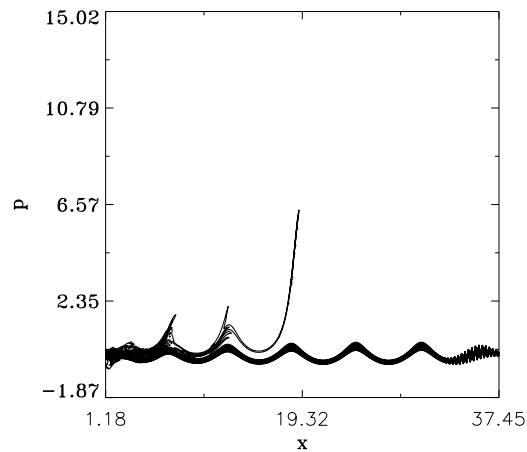


Figure 11: Phase-space contour plot of the electron distribution function at $t=38.33$ for the case with $T_e=0.4keV$, and a linearly polarized wave.

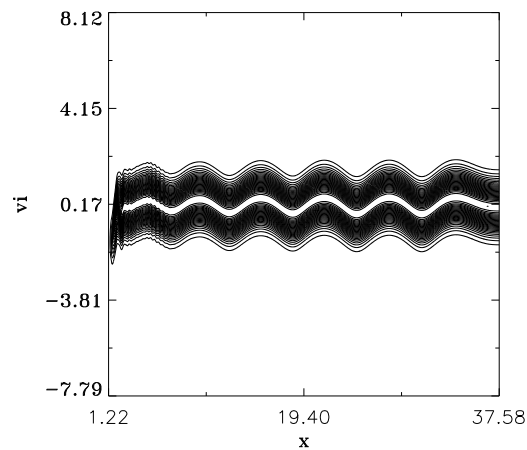


Figure 12: Phase-space contour plot of the ion distribution function at $t=38.33$ for the case with $T_e=0.4keV$, and a linearly polarized wave.

4 Conclusion

Simulations for the laser wake-field acceleration have been carried out using a 1D relativistic Vlasov-Maxwell equations. Both electrons and ions have been included in the present simulations. The method used for the numerical solution consists of integrating the Vlasov equation in two dimensions along its characteristics, using for interpolation a tensor product of cubic B -splines. This method has shown in previous applications to be accurate, to have little numerical diffusion, and to give accurate results in the low density region of the phase space [5, 10, 12, 13]. This is important since the physics of interest in the present problem is associated with localized low density beam structures which detach from the bulk and are accelerated in the low density regions of the phase-space. The

results in Section 3.1 for the circularly polarized wave show that the peak of the wake field immediately behind the laser pulse is in good agreement with the value calculated using the nonlinear relativistic cold plasma equations [1,2], and that the wake electric field peaks and the electron density peaks have a tendency to decrease away from the pulse, in contrast with the results of a cold plasma [1,2] where the peaks remain constant. This decrease appears to be caused by a finite temperature effect and is in agreement with the results reported in [7]. So even for rather high temperatures, the fields immediately behind the laser pulse are quite close to those of the cold fluid. For the cases studied with linear polarization, the density peaks behind the pulse as well as the wake fields peaks appear to be more uniform than the ones obtained for the circular polarization case. For the present set of parameters and time considered, we observe little deformation in the shape of the laser pulse as it propagates.

Acknowledgments

The author is grateful to the Centre de calcul scientifique de l'IREQ (CASIR) for computer time used to do this work. The constant support and interest of Dr. André Besner is gratefully acknowledged.

References

- [1] P. Sprangle, E. Esarey and A. Ting, Nonlinear interaction of intense laser pulses, *Phys. Rev.*, A41 (1990), 4463-4469.
- [2] A. Ting, E. Esarey and P. Sprangle, Nonlinear wake-field generation and relativistic focusing of intense laser pulses in plasmas, *Phys. Fluids*, B2 (1990), 1390-1394.
- [3] R. Bingham, J.T. Mendonca. and P.K. Shukla, Plasma based charged-particle accelerators, *Plasma Phys. Control. Fusion*, 46 (2004), R1-R23.
- [4] B.A. Shadwick, G.M. Tarkenton, E. Esarey and C.B. Schroeder, Fluid and Vlasov models of low-temperature, collisionless, relativistic plasma interactions, *Phys. Plasmas*, 12 (2005), 056710-1-056710-8.
- [5] D. Strozzi, M. Shoucri, A. Bers and E. Williams, Vlasov simulations of trapping and inhomogeneity in Raman scattering, *J. Plasma Phys.*, 72(6) (2006), 1299-1302.
- [6] S. Guérin, G. Laval, P. Mora, J.C. Adam, A. Héron and A. Bendib, Modulational and Raman instabilities in the relativistic regime, *Phys. Plasmas*, 2 (1995), 2807-2814.
- [7] J. Krall, G. Joyce and E. Esarey, Vlasov simulations of very-large-amplitude wave generation in the plasma wakefield accelerator, Naval Research Lab. Memorandum Report 6772 (1991).
- [8] C.Z. Cheng and G. Knorr, The integration of the Vlasov equation in configuration space, *J. Comp. Phys.*, 22 (1976), 330-351.
- [9] R. Gagné and M. Shoucri, A splitting scheme for the numerical solution of a one-dimensional Vlasov equation, *J. Comp. Phys.*, 24 (1977), 445-449.
- [10] F. Huot, A. Ghizzo, P. Bertrand, E. Sonnendrücker and O. Coulaud, Instability of the time splitting scheme for the one-dimensional and relativistic Vlasov-Maxwell system, *J. Comp. Phys.*, 185 (2003), 512-531.

- [11] M. Shoucri 2007a 'The method of characteristics for the numerical solution of hyperbolic differential equations', in *Computer Physics Research Trends* (Ed. Silvan J. Bianco, Nova Science Publishers Inc., NY), Chapter 1.
- [12] M. Shoucri, Eulerian codes for the numerical solution of the Vlasov equation, *Nonl. Sci. Num. Simul.*, 13 (2008), 174-182.
- [13] M. Shoucri, H. Gerhauser and K.H. Finken, Integration of the Vlasov equation along characteristics in one and two dimensions, *Comp. Phys. Comm.* 154 (2003), 65-75.
- [14] M. Shoucri, H. Gerhauser and K.H. Finken, Study of the generation of a charge separation and electric field at a plasma edge using Eulerian Vlasov codes in cylindrical geometry , *Comp. Phys. Comm.*, 164 (2004), 138-149.
- [15] E. Pohn, M. Shoucri and G. Kamelander, Eulerian Vlasov codes, *Comp. Phys. Comm.*, 166 (2005), 81-93.